THE ASTROPHYSICAL JOURNAL, 391:750–759, 1992 June 1

X-RAY TO INFRARED OBSERVATIONS OF THE CATACLYSMIC VARIABLE KO VELORUM (E1013−477)[1]

R. M. SAMBRUNA,[2] L. CHIAPPETTI,[3] A. TREVES,[2] J. M. BONNET-BIDAUD,[4] P. BOUCHET,[5]
L. MARASCHI,[6] C. MOTCH,[7] M. MOUCHET,[8] AND S. VAN AMERONGEN[9]
Received 1991 October 2; accepted 1991 November 27

ABSTRACT

Simultaneous photometric and spectrometric observations of the source E1013−477 in X-ray, UV, optical, and IR bands are presented. Evidence is found in support of the recently proposed orbital period of 10.12 hr. The X-ray spectra (0.1–10 keV) are well fitted by a single power law of photon index −0.8 with interstellar absorption $N_H \leq 10^{21}$ cm^{-2}. Discussing the classification of the source in the frame of the magnetic cataclysmic variables, we conclude that E1013−477 is probably a new intermediate polar candidate.

Subject headings: novae, cataclysmic variables — stars: individual (KO Velorum) — X-rays: stars

1. INTRODUCTION

The X-ray source E1013−477 was first detected by the *HEAO 1 A-2* experiment and subsequently better located by means of *Einstein* IPC observations. Its optical counterpart was identified as the 17th magnitude blue star KO Vel by Mason et al. (1982, 1983). In the latter reference, the authors proposed the classification of the object as an AM Her system on the basis of the strong, broad emission lines in the optical and UV spectra, and of the rapid flickering in the optical light curve. An orbital period of 103 minutes was proposed, based on the recurrence of dips in photometric observations taken in 1981 June and 1982 January. This period was not confirmed by observations in 1982 April. The proposed classification seemed to fail subsequently, due to the lack of polarization of the emitted radiation: Cropper (1986) found an upper limit of $1.0 \pm 1.3\%$ for circular polarization, well below the value usually detected for an AM Her system. However, the previous author suggested that E1013−477 is an AM Her object in a low state. After the earlier observations by Mason et al. (1983), the source faded to 19th magnitude, and no further observations in a bright state have been reported up to now (see below, § 4.1). In addition, the proposed orbital period of 103 min was not confirmed by later photometry and time-resolved spectroscopy in the optical band (Mouchet et al. 1987).

Further photometry in the *I* band (Mukai & Corbet 1987) gave some new hints about the nature of the source E1013−477. From evidence of periodicities at 6.4 hr and 71 minutes the authors were able to advance the possible classification of the source as an intermediate polar (IP) system. Additional arguments in favor of such a classification were given by the detection in the optical of three new coherent periods at 4.9 hr and 68 and 89 minutes (Kubiak & Krzeminski 1989). These were interpreted as the orbital, rotational, and beat period, respectively, a typical signature of an IP (Warner 1986).

The classification of E1013−477 is still a matter of debate. From the analysis of three CCD photometric sets of observations, Mukai & Corbet (1991; MC in the following) were able to deduce, convincingly, an orbital period of 10.12 hr. They also argued that all the previously found periodicities could be various harmonics or 1 day aliases of this fundamental period.

We observed E1013−477 in the X-ray band with the *EXOSAT* satellite in 1984 March. These are the only high-quality X-ray observations so far obtained, which allow a rather detailed spectral study. In this paper, we present these data (preliminarily reported at a conference; see Chiappetti et al. 1989, hereafter CMST), together with simultaneous UV data taken with the *International Ultraviolet Explorer* satellite (*IUE*) and optical and infrared observations obtained at ESO (see Maraschi et al. 1984 and Mouchet et al. 1987 for previous reports of some UV and optical-IR data, respectively).

The paper is organized as follows. In §§ 2, 3, and 4 we report observations and analysis of X-ray, UV, and optical-IR data, respectively. The results are summarized and discussed in § 5.

2. X-RAY DATA

2.1. *Observations*

E1013−477 was observed by the *EXOSAT* satellite on 1984 March 23 between 10:32 and 14:24 UT; details of observations are summarized in Table 1A. We used data from two of the instruments on board the satellite (for a detailed description of the experiments see White & Peacock 1988 and references therein).

The Low Energy imaging telescope (LE) operated in the soft X-ray band (0.02–2.5 keV). A photon counting Channel Multiplier Array, without intrinsic energy resolution, was located in the focal plane. Of the five filters interposed in the beam (offering broad-band spectral resolution), only thin Lexan (Lexan 3000 Å) was used.

The Medium Energy (ME) experiment consisted of eight

[1] Based on data obtained with the *EXOSAT* and *IUE* satellites and ESO telescopes.

[2] SISSA/ISAS, Strada Costiera 11, 34014 Trieste, Italy.
[3] IFCTR-CNR, via Bassini 15, 20133 Milano, Italy.
[4] Service d'Astrophysique, CEN-Saclay, DPh/SAp, F-91191 Gif-sur-Yvette Cedex, France.
[5] ESO, La Silla Observatory, La Serena, Chile.
[6] Sezione di Astrofisica, Dipartimento di Fisica, via Celoria 16, 20133 Milano, Italy.
[7] CNRS, Observatoire de Haute-Provence, F-04870 Saint-Michel l'Observatoire, France. Presently at Max-Planck-Institut für Physik und Astrophysik, Institut für extraterrestrische Physik, W-8046, Garching bei München, Germany.
[8] Observatoire de Paris-Meudon, 5 Place J. Janssen, F-92195 Meudon, France and Universite' de Paris 7, 2 Place Jussieu, F-75251 Paris Cedex, France.
[9] Astronomical Institute "Anton Pannekoek," University of Amsterdam, Roetersstrat 15, 1018 WB Amsterdam, The Netherlands.

TABLE 1

JOURNAL OF OBSERVATIONS

A. X-RAY OBSERVATIONS

Telescope	Start Date	Start Time (U.T.)	End Time (U.T.)	Exposure Time (s)
LE + 3000 Lexan	1984 Mar 23	10:32	14:24	9462
ME	1984 Mar 23	10:32	14:24	14780

B. UV OBSERVATIONS

Camera/Image Number	Start Date	Start Time (U.T.)	End Time (U.T.)	Exposure Time (s)
SWP 22553	1984 Mar 23	04:30	07:50	12000
LWP 03016	1984 Mar 23	07:54	10:40	9960

C. OPTICAL AND INFRARED OBSERVATIONS

Telescope	Start Date	Start Time (U.T.)	End Time (U.T.)	Exposure Time (s)	Notes
SPECTROSCOPY					
IDS (3.6 m ESO).....	1984 Mar 29	00:14	04:27	60	200 spectra
	1984 Mar 30	01:58	03:52	300	8 spectra
				600	12 spectra
PHOTOMETRY					
Fast photometry	1984 Mar 23	03:15	03:57	60	For each filter, *UBVRI*
(1.54 m Danish)	1984 Mar 24	01:23	03:23	...	*V*, time resolution 0.1 s
	1984 Mar 24	01:19	03:27	60	For each filter, *UBVRI*
IR (3.6 m ESO)	1984 Mar 24	02:35	03:46	...	*JHK*

Argon filled proportional counters, sensitive in the 1–20 keV energy range. They were grouped to form two panels ("halves"). During the observations, one half was pointing toward the source ("aligned half"),[10] while the other monitored the sky ("offset half"), giving an independent background estimate.

For the LE experiment, we measured the counts in a 5×5 pixel (1 pixel = 4″) box around the source position and subtracted the background determined in an outer region. The net counts are 42.7 ± 9.4 for an effective exposure time of 9462 s. The count rate, after correction for dead times, point spread function, background nonuniformity, and vignetting is $(4.5 \pm 0.9) \times 10^{-3}$ counts s^{-1}.

For the ME experiment there is signal from the source in the PHA channel range 10–35 (2–9 keV), amounting to 0.46 ± 0.05 counts s^{-1} $half^{-1}$ for an exposure time of 14780 s.

2.2. *Timing Analysis*

A look at the LE data showed that, due to the limited number of photons, any timing analysis is forbidden. Thus, such analysis was performed using the ME data only. In Figure 1*a* we show the ME net light curve in the 2–9 keV energy range. The low statistics do not allow any splitting in further energy ranges, e.g., for a hardness ratio analysis.

A Fourier analysis (Ferraz-Mello 1981) has been applied to the light curve without background subtraction and also to the background alone, for reference. We are able to exclude the presence of any of the periods proposed in the literature, shorter than the duration of the observations (see Table 1A), as well as of any other coherent periodicity with a chance probability smaller than 0.1%, the typical value of background fluctuations. We have also performed a folding analysis (Scargle 1982); a search in the range 60–120 minutes does not find any modulation. The light curves folded at the proposed periods do not contain any clear evidence of modulation (see Figure 2 of CMST). Note, however, that we are unable to verify the period proposed by MC, which is too long with respect to the duration of our X-ray observations.

In order to strengthen our conclusion, we have performed a simulation by Monte Carlo techniques, generating light curves with a similar background noise level and with a sinusoidal component of decreasing amplitude. We find that we would be able to detect any period (at a significance greater than 0.999) up to an amplitude of 0.15 counts s^{-1}, corresponding to a pulsed fraction greater than 30% (we define the pulsed fraction as the ratio of the area of the pulsed part of the light curve, i.e., above the minimum, to the total area under the light curve).

2.3. *Spectral Analysis*

2.3.1. *ME Data*

In order to derive the net spectrum we carefully examined the spectra obtained by the satellite in the slew manoeuvres and pointing. The slew-in data were not used, due to their short duration and to the large variability of the particle background. Then the net spectrum was obtained by subtracting from the gross spectrum the background measured by the same half during the slew-out manoeuvre. The background in the other half was found to be constant from the pointing to

[10] All count rates given in the text and figures refer to the on-source half experiment; this is indicated by the notation counts s^{-1} $half^{-1}$.

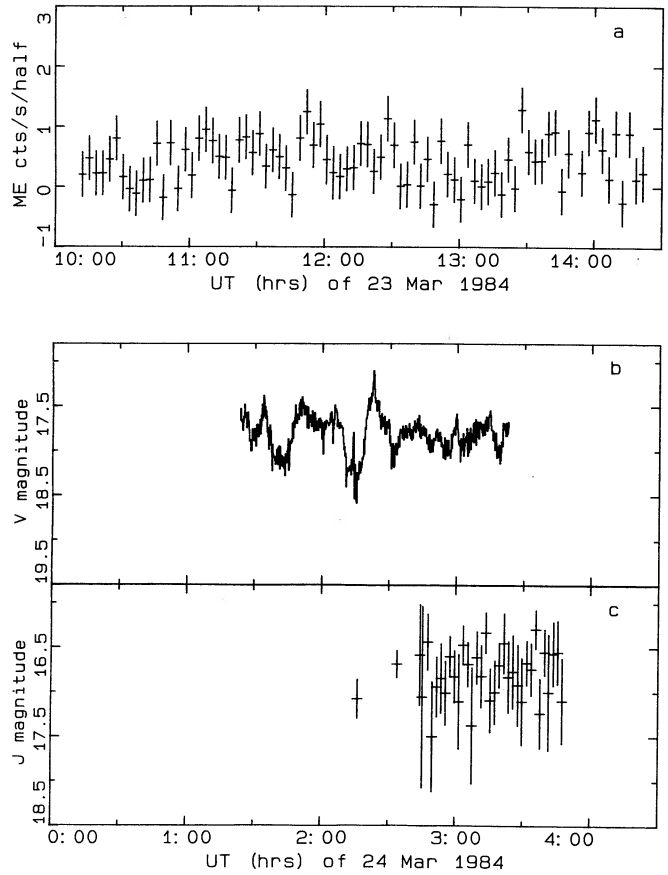

FIG. 1.—Light curves of E1013−477, (*a*) in X-rays (2–9 keV; 1984 March 23), (*b*) in the *V* band, and (*c*) in the *J* band (1984 March 24).

the slew-out phase. The net spectrum was rebinned so that in each new bin the signal is at least at the 3 σ level. The fitting of these data, because of their limited statistical quality, can constrain the free parameters only rather poorly. This is clearly seen in Table 2, top, where the results of fits with a bremsstrahlung distribution and a power law (best-fit values, 90% confidence intervals, and χ^2) are reported. The power law is preferred to the thermal model on the basis of the better χ^2 (7.6 and 9.4, respectively, for 7 degrees of freedom).

2.3.2. *LE + ME Data*

Assuming that a single spectral component is responsible for the emission in the soft and hard X-ray bands, we attempted a joint fit to the LE and ME data together. In Table 2, *bottom*, we list the results of fits with a bremsstrahlung distribution and a power law. Again, the latter model fits the data better. In Figure 2, the photon spectrum, deconvolved with the best-fit power-law model, is shown while the inset depicts the confidence contours at the 68%, 90%, and 99% levels. As can be seen clearly from Table 2, *bottom*, and from the inset of Figure 2, the joint fit allows us to constrain the column density to a very small value (formal best fit at 10^{19} cm^{-2}) and in a 90% confidence interval ($\leq 9 \times 10^{20}$ cm^{-2}), narrower than that found for the ME spectrum only (Table 2, *top*).

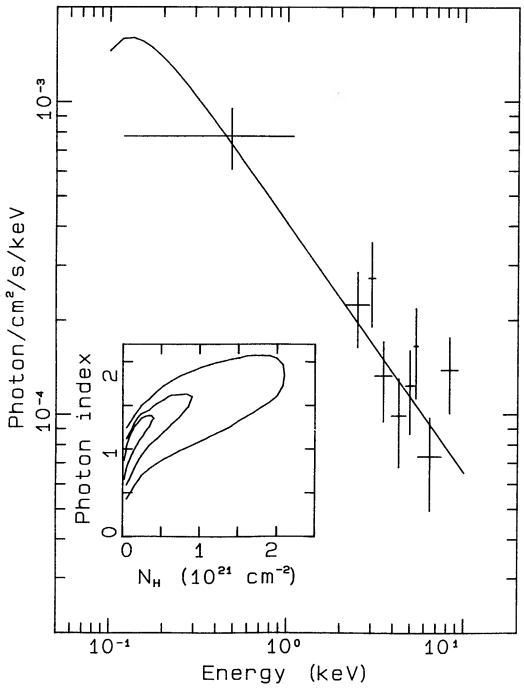

FIG. 2.—The photon spectrum of E1013−477 deconvolved with the best-fit power-law model. The first data point is the LE measurement. The inset shows the confidence contours at the 68%, 90%, and 99% levels.

2.3.3. *Distance to the Source*

We were able to determine an upper limit to the distance of E1013−477 from our X-ray data. Using our 90% confidence contour value of the hydrogen column density and the map of the local distribution of hydrogen (Paresce 1984), we found that the source is no more distant than ~150 pc (the direction

TABLE 2

SUMMARY OF X-RAY SPECTRAL FITS

Model	Photon Index[a]	kT[a] (keV)	N_H[a,b] ($\times 10^{21}$ cm^{-2})	χ^2	D.O.F.
FIT TO ME DATA					
Bremsstrahlung	...	>5.4	<70	9.4	7
Power law	0.7 (<1.5)	...	0.1 (<0.9)	7.6	7
FIT TO LE + ME DATA					
Bremsstrahlung	...	>10	0.7 (0.4–1.3)	10.3	8
Power law	0.8 (<1.6)	...	0.01 (<0.9)	7.6	8

[a] For photon index, kT, and N_H, values are best fit and 90% confidence intervals.
[b] N_H are calculated with the cross sections of Morrison & McCammon (1983).

toward E1013−477 crosses a relatively thick region in the Galactic plane).

From our LE + ME best fit, we estimated a flux (at the source, in the 0.1–9 keV energy band) of $7.6^{+2.4}_{-0.5} \times 10^{-12}$ ergs cm^{-2} s^{-1} (given with 90% confidence limits). This flux implies a luminosity $L_X = 2 \times 10^{31}$ ergs s^{-1}, using the value of 150 pc for the distance.

2.3.4. *Comparison with Previous Measurements*

We have compared the X-ray intensity of the source with that found previously by other missions (*HEAO 1*, *Einstein*), as reported by Mason et al. (1983). The fluxes were calculated in the operational energy bands of these satellites (CMST). We found that the source in 1984 was substantially fainter by a factor of 100 than in 1977 (*HEAO 1* observations), but stronger by a factor of 5 than in 1979–80 (*Einstein* observations). Note, however, that there is some uncertainty of the identification of the *HEAO 1* source with E1013−477, because of the proximity, in the *Einstein* IPC image, of two other sources (a K0 star and a quasar; Mason et al. 1983).

Note that all fluxes given in Mason et al. (1983) were computed assuming a $kT \approx 1$ keV which is clearly inconsistent with our fits (see above). We have also compared our spectral parameters with those derived from the analysis of the previous observations. Little can be said about the spectrum based on the single *Einstein* IPC point. The ratio of the count rates in the high- and low-energy *HEAO 1* bands given in Mason et al. (1983) implies (see Fig. 7 of Nugent et al. 1983), for any value of the absorption, a spectrum steeper than 1.5 (or a bremsstrahlung temperature lower than 2 keV). Therefore, we can conclude that the *HEAO 1* spectrum is definitely softer than ours.

3. UV SPECTRA

3.1. *Observations*

Low-resolution ultraviolet spectra of E1013−477 were obtained with *IUE* (Boggess et al. 1978) in the 1200–1980 Å and 1900–3200 Å bands (SWP and LWP cameras) on the same day as the X-ray ones. As can be clearly seen in Table 1B, the UV and X-ray observations were not strictly simultaneous. The line-by-line spectra, generated from the raw image with the standard *IUE* Spectral Image Processing System, were all processed with the Gaussian extraction method described by Urry & Reichert (1988) and implemented by us within the context of the ESO IHAP software package. This method determines a variable pseudo-slit width and a local background by preliminary fitting, over wide wavelength intervals, the intensity distribution perpendicular to the dispersion with a Gaussian plus a linear trend. The procedure objectively rejects regions where the signal is too weak or the background too noisy. The spectrum obtained is plotted in Figure 3.

In order to perform a spectral fitting, continuum points were measured averaging the flux in intervals of 50 Å in selected line-free regions. The errors, used for fitting, are purely the statistical ones and are, therefore, underestimated.

3.2. *Spectral Analysis*

We have considered first the SWP spectrum. These data were best fitted with a power law reddened with the extinction curve of Seaton (1979). The fit to the data with A_V free, gives for the reddening a value consistent with zero. We also performed the fit with A_V fixed to zero. The results of the fits are reported in Table 3 together with those obtained by analogous fits to the SWP + LWP data (first two entries in Table 3). In Figure 4, top panel, we plot the SWP + LWP data (*diamonds*). The lines labeled "a" and "b" are the fits to the SWP + LWP data and to the SWP data only, respectively, with A_V fixed to zero. It is apparent that the LWP data lie above the latter line. In addition, the χ^2 of the SWP + LWP data fit is larger than that of the fit to the SWP data only. Of course, one cannot exclude, a priori, that this effect is caused by variability, although a look at Table 1B shows that this is unlikely due to the length of the exposure times. Therefore, we conclude that a single power law is insufficient to fit both SWP and LWP data *together*.

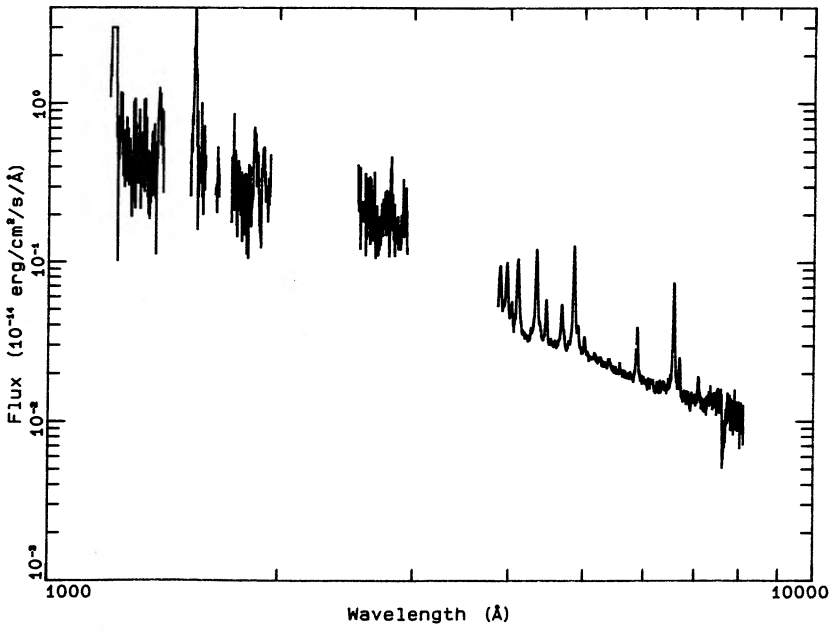

FIG. 3.—The UV (March 23) and optical (March 29) average spectrum of E1013−477

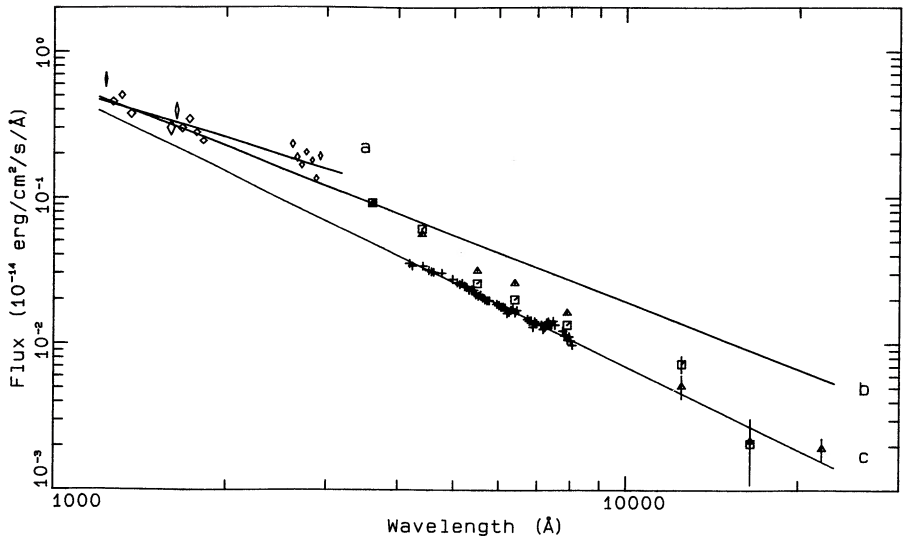

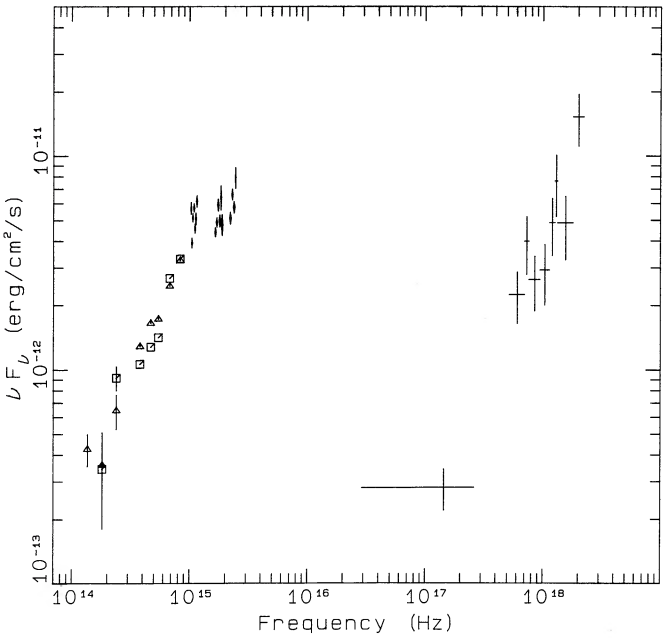

FIG. 4.—*Top panel*: UV and optical energy distribution of E1013−477. Diamonds indicate 50 Å averages of the March 23 UV spectrum (see Fig. 3) taken in line-free regions. The squares and triangles represent *UBVRIJHK* photometry taken on March 24 (different symbols correspond to different sets of measurements in the same night). Crosses indicate the 50 Å averages of the March 29 optical spectrum (see Fig. 3) taken in line-free regions (note that significant contamination due to Balmer continuum and line contamination is present in the *U* and *B* bands). Solid line labeled (a) indicates: the best fit to the UV (SWP + LWP) data points; line (b), the best fit to the UV SWP data points, extrapolated also to optical wavelengths; and line (c) the best fit to the March 29 optical data points, extrapolated to UV and IR wavelengths.

Bottom panel: overall energy distribution of E1013−477, showing X-ray (LE and ME) data (March 23; *error bars*) UV data (March 23; *diamonds*), optical-IR photometry data (March 24; *triangles and squares*, two separate measurement sets obtained during same night).

Our data have been compared with the 1982 January UV spectra (Mason et al. 1983). We reduced and analyzed the latter data, retrieved from *IUE* VILSPA archives, using the method described above and obtained the results listed in Table 3, the first three entries. As can be seen, the fit to the 1982 data provides power-law indexes which are systematically higher than those provided by fits to our data. Two main conclusions can be derived from the inspection of Table 3. First, both the 1982 SWP and LWP spectra are well fitted by a single power law, contrary to the 1984 case. Second, the 1982 spectrum is steeper than the 1984 one.

4. OPTICAL DATA

4.1. *Observations*

Photometric (*UBVRI*) and spectroscopic data in the optical band were taken on 1984 March 23–24 and 29–30, respectively, at ESO La Silla, Chile. Details of observations are reported in Table 1C. Red (RI) magnitudes are from the Cousins system (Bessell 1979).

March 23 *UBVRI* measurements were not used due to bad observing conditions. March 24 *V* and *J* light curves are shown in Figures 1*b–c*, from which strong variations in the *V* band are apparent. Note that the source is found in a optical level higher ($V \sim 17.7$–18) than that found ($V = 19$) in the observations after those of Mason et al. 1983. Because of the short duration of the observations, we are unable to confirm, with any statistical significance, the periods proposed in the literature.

Spectral measurements were obtained on March 29 and 30 at ESO (La Silla, Chile) using the Boller and Chivens spectrograph and the Image Dissector Scanner mounted on the 3.6 m telescope (see Table 1C). On March 29 long series of consecutive spectra covering the wavelength range from 4000 to 7900 Å were obtained at a dispersion of 224 Å mm^{-1} (19 Å FWHM resolution), with integration times of 1 minute. On March 30, 8 spectra of 5 minutes, then 12 spectra of 10 minutes were taken at a dispersion of 114 Å mm^{-1} (9 Å FWHM resolution) covering the range 4300–6700 Å. The data were calibrated in wavelength and corrected for extinction after sky subtraction in a standard way with an accuracy of 15%. Figure 3 shows the mean of the spectra from the March 29 observations.

Analysis of the continuum and of the lines have been separated in the following for clarity. In the optical spectrum, emission lines such as the Balmer lines, He I, and He II are found.

Radial velocity measurements from Hα and Hβ emission lines were obtained from the analysis of the 38 rebinned

TABLE 3

SUMMARY OF ULTRAVIOLET (*IUE*) SPECTRAL FITS: POWER-LAW MODEL

DATA	A_V FREE			A_V FIXED (=0.0)		
	Wavelength Index	A_V	$\tilde{\chi}^2$	Wavelength Index	$\tilde{\chi}^2$	D.O.F.
1984 SWP	1.5	≤ 0.01	3.8	1.5	3.2	9
1984 SWP + LWP	1.4	0.23	6.5	1.2	5.8	16
1982 SWP[a]	...	...	...	2.5	1.5	9
1982 SWP + LWP	1.4	0.01	7.5	1.5	6.3	15

[a] Unable to constrain the fitting parameters for A_V free.

spectra of March 29 and of the individual spectra of March 30. Note the relatively short duration of the data (4 hr) in each night. We can combine the data of both nights for each line, since the single observing run of 4 hr is too short to allow a study of the longest periods proposed in the literature, in particular that of 10.12 hr found by MC.

4.2. *Radial Velocities*

Sinusoidal fits to radial velocity curves give periods for both Hα and Hβ lines very close to the period of (10.12 ± 0.07 hr) found by MC (hereafter referred to as P_{MC}). From these preliminary fits, we deduce that a sinusoid with a period consistent within the errors with P_{MC} can describe the behavior of the radial velocity changes.

The uncertainty on P_{MC}, when propagated to the epoch of our observations, gives an error of 12.4 cycles. Hence, we are unable to make a relative phasing of MC photometry with our radial velocity curves.

Figure 5*a* and 5*b* show phase-resolved radial velocity curves for Hα and Hβ lines, respectively. Data taken on 29 March are plotted with filled squares, while crosses refer to data taken on the following night. These data were fitted by a sinusoidal law $A_1 + A_2 \sin \alpha$, where $\alpha = 2\pi(A_3 + \phi)P^{-1}$, with the phase given by ϕ and the period by P. We fixed $P = P_{MC}$ and obtained for the free parameters A_1, A_2, A_3 the best fit values given in the caption of the figures. The best-fit sinusoids are overplotted on the data in Figure 5.

A folding search analysis has been done both for Hα and Hβ. Three peaks are found, corresponding to the following periods: $P_1 = 18277$ s, $P_2 = 25687$ s, and $P_3 = 36555$ s. Their meaning is clear: P_3 is very close to P_{MC}, P_1 is its first harmonic, and P_2 the 1 day alias. We found, however, that a large uncertainty is related to P_3 (a very wide peak).

In addition, a Fourier transform of the data has been performed, using the Ferraz-Mello (1981) method. The results obtained for the Hα and Hβ lines are shown in Figure 6. Vertical bars indicate the reference periods quoted above, P_1, P_2, P_3. Again, three peaks are found in rather good agreement with these periods. In order to check the significance of these peaks the spectral windows have been computed and normalized to the power of the P_3 peak. This comparison shows clearly that P_1 and P_2 are due to window effects. If the spectral window is normalized, instead, to the P_1 peak it still reproduces the shape and position of the other two peaks but the predicted power turns out to be in excess over the data. Since this is meaningless it is clear that P_{MC} is preferred to its 1 day alias P_1. The chance probability of P_{MC} is found to be of the order of 2×10^{-9} and 5×10^{-9} for Hα and Hβ, respectively.

In summary, from the above analysis, we conclude that our data are consistent with the proposed period of 10.12 hr. However, the uncertainty of the observed period and, thus, of the number of related cycles does not allow any relative phasing of our radial velocity curves with the previous photometric results.

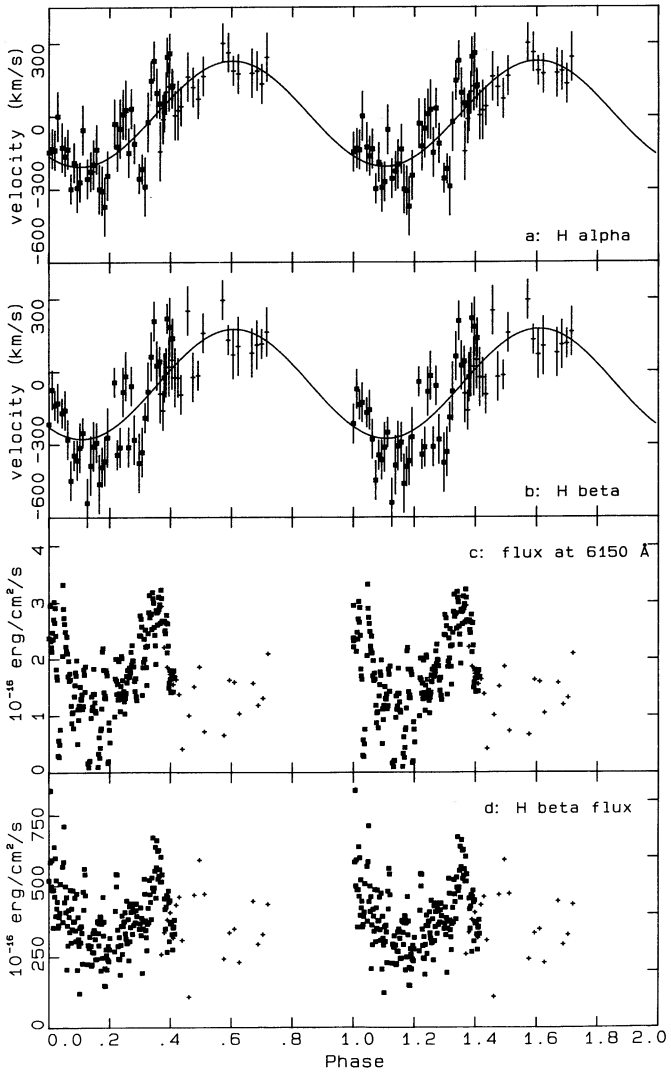

FIG. 5.—The following data are reported folded at P_{MC} (two cycles shown for clarity): (*a*) Hα radial velocity, (*b*) Hβ radial velocity, (*c*) continuum flux in the range 6100–6200 Å, and (*d*) flux in the Hβ line. Squares and crosses correspond to the March 29 and 30 observations, respectively. Individual exposures are shown for fluxes, while for radial velocity averages over 5 spectra are shown. For radial velocity the best fit sinusoid (with period fixed to P_{MC}) is also shown with the following parameters; for Hα: $A_1 = 10$ km s^{-1}, $A_2 = 216$ km s^{-1}, and $A_3 = 0.148$; for Hβ: $A_1 = -52$ km s^{-1}, $A_2 = -226$ km s^{-1}, and $A_3 = 0.142$ (see text).

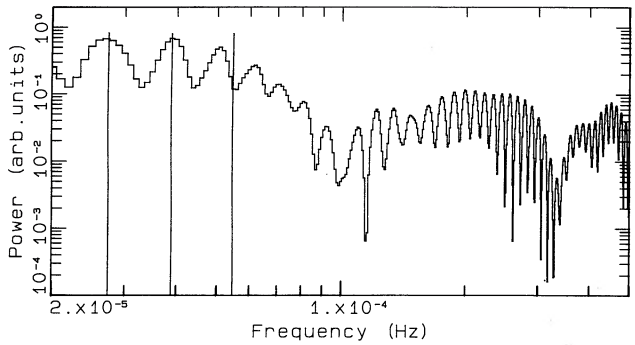

FIG. 6.—Periodogram of the Hα radial velocity (according to Ferraz-Mello 1981). The three fiducial marks indicate, from left to right, P_{MC}, the 1 day alias of P_{MC}, and the first harmonic of P_{MC}. The modulation due to the spectral window can be clearly seen.

4.3. *Continuum Analysis*

4.3.1. *Timing Analysis*

We consider only data from the March 29 observations, for which the time coverage is ~4 hr (Table 1C). Observations taken on March 30 do not have sufficient coverage and data points to allow a detailed time analysis. Flux values were measured as a function of time for five selected, 100 Å wide line-free regions of the optical continuum. They were estimated by an automatic procedure from the individual spectra.

Periodograms of the selected light curves were computed using the Ferraz-Mello (1981) method. Table 4 gives the principal peaks found in the periodograms and their significance (chance probability). The peak at 25 minutes is an instrumental effect (there is a systematic change in IDS data storage process every 25 minutes). Two peaks at 19 minutes and 98 minutes are found in each case (the 98 minute period is not seen in the periodogram at 4200 Å) with a chance probability less than 10^{-2} and 6×10^{-4}, respectively.

With the above definition of the pulsed fraction (see § 2.2), we found the values reported in Table 4, in order of increasing wavelength. It is apparent that the pulsed fractions increase with the wavelength, except for the 7300 Å value.

In order to improve the significance of the analysis, we have combined the data for the two nights. Note, however, that besides the different time coverage, the two sets of data differ also in the exposure times (Table 1C). We performed the same temporal analysis as above. In the periodograms we found two significant peaks at 19 and 98 minutes with a chance probability less than 10^{-5} and 10^{-4}, respectively. The 98 minute period is close to the 103 minute one detected by Mason et al. (1983). No peaks at P_{MC} are present. Moreover, the combined light curves folded at P_{MC} do not show any evident trend (Fig. 5*c*), hence, we cannot make any obvious phasing between the radial velocity curves and the fluxes.

TABLE 4

OPTICAL CONTINUUM TIMING ANALYSIS

λ (Å)	P (min)	Chance Probability	p.f.
4200.....	19	9×10^{-3}	9%
	25	8×10^{-7}	
4560.....	19.2	1×10^{-5}	14%
	25.2	2×10^{-3}	
	98	2×10^{-4}	
5200.....	18.9	1×10^{-5}	20%
	98	1×10^{-4}	
6150.....	18.9	1×10^{-5}	25%
	25	1.5×10^{-3}	
	98	2×10^{-4}	
7300.....	18.9	6×10^{-8}	22%
	26	2×10^{-4}	
	92.6	6×10^{-4}	

NOTE.—p.f. = pulsed fraction, see text for definition.

4.3.2. *Overall Energy Distribution*

An energy spectral analysis was performed to the data of March 23, fitting line-free regions of the average optical continuum (Fig. 3) with a power law ($F_\lambda \propto \lambda^{-\alpha}$), yielding the best fit value $\alpha = 1.9$. The *UBVRIJHK* data obtained on March 24 have qualitatively the same trend as the March 23 spectral data points. In addition, the match between the spectrum and the VRI points is indicative of the night-to-night variability in the overall flux level. We then use the photometric data to create an overall energy distribution from infrared to ultraviolet, which is plotted in Figure 4*a*, top panel. The line labeled "c" is the fit to the March 29 average optical continuum extrapolated backward into the UV band. One can see that ultraviolet data points, in particular at longer wavelengths, lie above this line. The data points corresponding to the measurements in the *U* and *B* bands also lie above the line, but this can be attributed to Balmer continuum and line contamination. The line labeled "a" is the fit (see § 3.2) to SWP + LWP data, while that labeled "b" is the fit to the SWP data only, extrapolated into the optical region.

Two general remarks can be made about the composite spectrum. We can distinguish at least two main components in the overall energy distribution: a power law in the infrared-optical and ultraviolet (short-wavelength) regions, and a "bump" in the far UV. If we add the X-ray data points a further component is introduced, as shown in the Figure 4*b*, bottom panel.

There are no evident features of a secondary star in the energy distribution. This might suggest a very cold main-sequence star. The possible nature of the secondary is, however, discussed in MC. More observations are therefore needed, in particular in the infrared band, to fully understand this point.

4.4. *Emission-Line Analysis*

The main lines found in the average optical spectrum are listed in column (1) of Table 5. Some of the lines, e.g., He II

TABLE 5

EMISSION-LINE EQUIVALENT WIDTHS AND FLUXES

	1984 Mar 29		1984 Mar 30	
LINE (1)	EW (Å) (2)	Flux ($\times 10^{-16}$) (ergs cm^{-2} s^{-1}) (3)	EW (Å) (4)	Flux ($\times 10^{-16}$ (ergs cm^{-2} s^{-1}) (5)
Hα	153	239	189	272
Hβ	93	302	144	347
Hγ	84	325	...	...
He I λ4471	13	43.9	22	61.6
He II λ4686	31	92.2	37	91.9
He I λ5875	26	52.8	43	68

NOTES.—Hβ is a blend of Hβ + He I λ4921 and He II λ4686 is a blend of He II + C III + N III + He I λ4713.

λ5411 and the blend C III–N III, are very weak in the average spectrum, although clearly detected in some individual spectra. Most of the strongest lines (Hβ, He II λ4686) are blended and this prevents us from determining a correct FWHM or FWZI. However, the radial velocity measurements are reliable since the lines which could affect them are weak compared to Hα and Hβ and are on the outer parts of the wings.

In columns (2) and (4) of Table 5 are reported the equivalent widths (EW) of the lines for the two nights and in columns (3) and (5) their intensities (in units of 10^{-16} ergs cm^{-2} s^{-1}). Line strengths are usual for cataclysmic variables (e.g., Echevarria 1988). We note that the EW, in particular for the Hβ line, are exceptionally stronger than the usual values found for magnetic systems (see, e.g., Patterson 1984). They compare well with the measurements of Mason et al. (1983) for the 1983 optical spectrum.

We measured intensities as a function of time for Hα and Hβ lines for both nights. We performed the same temporal analysis as for the continuum, as described in § 4.3, i.e., the Fourier transforms and the folding of the data both for the first night and the two nights combined. In the periodograms we did not find any significant peak at P_{MC} nor at any other periods. The folding at P_{MC} again does not show a clear trend (Fig. 5*d*).

5. DISCUSSION

In this section we address the still open question of the classification of E1013−477, reconsidering it in light of our results.

E1013−477 was classified as a magnetic cataclymic variable on the basis of its photometric and spectroscopic behavior in optical and UV bands. No direct evidence for the presence of a magnetic field has been detected (see § 1). The X-ray luminosity of the source compares well with that of dwarf novae systems and nova-like objects (Cordova & Mason 1983), but also with that of few IPs (Berriman 1988). In addition, the EW of the emission lines in the optical spectrum (see Table 5) are consistent with those found for some nonmagnetic CVs (Echevarria 1988). The possibility exists that E1013−477 is a nonmagnetic system. However, in favor of a magnetic nature is its strong X-ray emission in *both* soft and hard X-ray bands. In fact, it seems that most nonmagnetic CVs are weakly or not detected in the LE (van der Woerd 1987). Soft X-ray emission is observed in dwarf novae and nova-like objects only during outbursts (Cordova, Jensen, & Nugent 1981). In addition, the high-excitation emission lines of metals and in particular the strong He II λ4686 emission line exhibited by the source are not usually present in dwarf novae (Voikhanskaja 1987) nor in nova-like objects at minimum light (e.g., MV Lyr; Voikhanskaja 1988). The X-ray properties, discussed below, are better understood in the framework of a magnetic system, which we shall therefore assume.

In this context, the only options for a more detailed classification are the AM Her systems, characterized by synchronous rotation of the white dwarf with the orbital motion, and the IP and the DQ Her systems, which are nonsynchronous rotators. The DQ Her class contains two objects only: DQ Her itself and AE Aqr (Warner & Wickramasinghe 1991), which are both characterized by a short rotational period of the white dwarf (71 and 33 s, respectively). This period is around tens of minutes in the IPs. Thus, the short time variability is one of the observational tools to discriminate among these three classes of objects.

In our photometry (optical and X-ray data) there is no clear signature for periodicity. The only firm evidence is found in the radial velocity curves of the Hα and Hβ emission lines, which supports the orbital period of 10.12 hr proposed by MC. This value of the orbital period seems to rule out the hypothesis that E1013−477 is an AM Her system. In these systems, in order to achieve the spin-orbit coupling, the magnetic field B must be higher as the orbital period is longer. For instance, in the context of the model described by Lamb & Melia (1987) and illustrated in Figure 9 of their paper, the required value for B is 10^9 G, for a white dwarf radius of 10^9 cm, corresponding to a typical mass of 1.2×10^{33} g (Bailey 1991). This value is slightly larger than the highest values found for isolated magnetic white dwarfs ($\sim 5 \times 10^8$ G, Schmidt 1989). For such highly magnetized binaries, the bulk of the cyclotron emission would be shifted in the UV, and no polarization is expected in the optical. Besides, they would be strong UV emitters with a steep continuum. Bond & Chanmugam (1982) have failed to identify such systems, on the basis of these observational criteria. However, note that very few high magnetic field cataclysmic binaries are expected to be observed since they are thought to evolve very quickly and disappear as semidetached systems (Hameury, King, & Lasota 1989).

The analysis of the X-ray energy distribution gives another important finding. A single, hard component is found for the X-ray spectrum. This is inconsistent with the hypothesis of an AM Her object; this class is indeed characterized by a strong, soft X-ray blackbody emission and a hard X-ray bremsstrahlung component, which is generally weaker, although expected to be comparable, to the soft X-ray one in the standard model (see, e.g., Lamb 1985). On the contrary, the X-ray spectrum of E1013−477 is well fitted from the soft to the hard X-ray bands by a power-law model with a photon index consistent with ~ 1.4, a value usually found for most IPs in the hard X-ray band (Warner 1983; Schrivjer *et al.* 1985) and in the soft + hard X-ray bands (Szkody 1986).

The long-term X-ray behavior of E1013−477 suggests another argument against the AM Her hypothesis. As we have seen in § 2.3.4, the source X-ray intensity at the epoch of the *EXOSAT* observations was found to be a factor 100 less than at the earlier *HEAO 1* observations. Moreover, the *EXOSAT* spectrum was found to be harder than the *HEAO 1* spectrum. This behavior is inconsistent with that of the AM Her objects, which are expected to have harder X-ray emission in a *high* state (e.g., Lamb & Masters 1979).

We consider now the possibility that the system is a DQ Her or an IP. Even if the available data do not allow us to firmly establish the spin period of E1013−477, we can get an indication of its expected value on the basis of the work of Barrett, O'Donoghue, & Warner (1988) and Warner & Wickramasinghe (1991). These authors found a rather well defined correlation between the orbital and the spin periods for the magnetic cataclysmic variables. Assuming first that E1013−477 is an IP, from Figure 1 of Warner & Wickramasinghe (1991) we extrapolated a $P_{spin} = 66.8$ min, very close to some previous findings (see § 1). In this context, our detected periodicity of ~ 98 minute (see § 4.3.1) could be accounted for. Another possibility is that the source is a DQ Her system. In this case, a spin period around 33 s would be implied by analogy with AE Aqr, which has a period very close (9.9 hr) to that of E1013−477. No evidence has been found up to now in the literature for such a short period. Therefore, it seems that an IP classification may be relevant. We note that in this context, the lack of circular polarization seems a feature common to most IPs (Warner 1983; Berriman 1988).

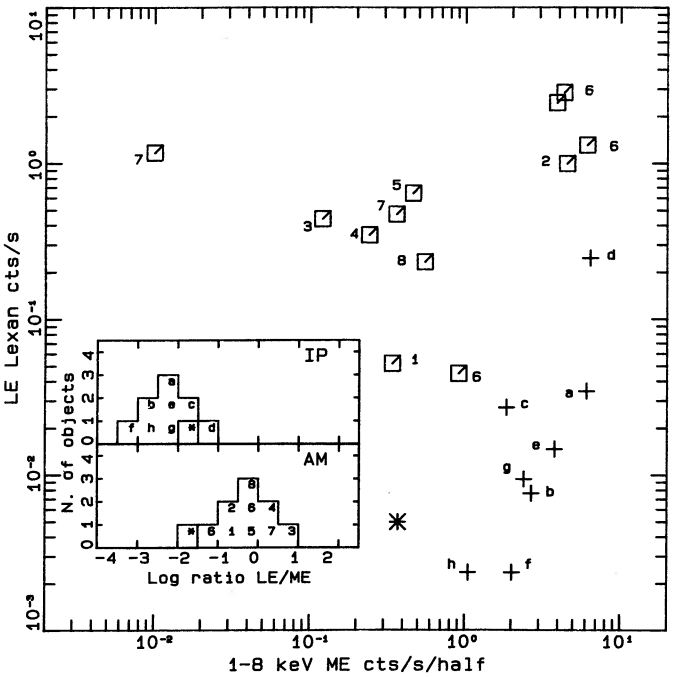

FIG. 7.—Main panel, soft (LE) and hard (ME) X-ray intensity of AM Her objects (*squares*) and intermediate polars (*crosses*), as obtained from the *EXOSAT* data base. The asterisk marks the position of E1013−477. AM Her objects (note that for some objects more than one measurement exists) are identified by numbers as follows: (1) BL Hyi = 0139−681; (2) EF Eri = 0311−277; (3) VV Pup; (4) AN UMa; (5) V834 Cen = 1405−451; (6) AM Her; (7) QQ Vul = 2003+225; (8) ST LMi = 1103+254. Intermediate polars (IP) are identified by letters as follows: (a) GK Per; (b) TV Col = 0526−328; (c) TW Pic = 0534−581; (d) EX Hya; (e) V1223 Sgr; (f) FO Aqr = 2215−086; (g) AO Psc = 2252−035; (h) BG CMi = 0729+103. The inset shows another view of the distribution of the LE/ME count rate ratio for AM Her objects (*lower inset panel*) and IPs (*upper inset panel*). Objects are identified by number/letters as in the main panel. E1013−477 is shown in both panels, in the box marked with the asterisk.

The long-term optical behavior of the source is an additional evidence in support of the claimed IP classification. In fact, E1013−477 has faded in the V band by ~ 2 mag over the period 1982 April–1984 March. Other IPs are known to exhibit similar behavior (Warner 1983; Garnavich & Szkody 1988).

In order to further enquire on the nature of the object, we have compared the soft and hard X-ray emission of the source with that of the other magnetic CVs. To this end, we have searched in the *EXOSAT* data base (*EXOSAT Observatory* 1991) for the LE and ME count rates of all the observed magnetic systems, retaining only ME observations with a quality flag of 3 or greater (on a scale 0–5). The results of our search (preliminarily reported in CMST) are shown in Figure 7, where we have plotted the LE count rates versus the ME ones, while the inset shows the corresponding histogram. From the figure, one can clearly see that the AM Her objects are separated from the IP. In fact, the AM Her systems lie in the upper half of the diagram, while the latter group of objects occupy the lower right corner. E1013−477 is found in this part of the diagram.

Beuermann (1988) has done, independently, a similar analysis for the AM Her objects only. An inspection of his Figure 2 shows that the AM Her objects occupy the upper half of the diagram, as we have found. In addition, Beuermann plots a line representing the contribution to the soft X-ray count rates given by a bremsstrahlung spectrum only. The AM Her systems observed in low states are not found below this line. In our plot the line would sharply divide the AM Her from the IP objects, that is, the objects with a hard and soft X-ray component (polars) from those with a hard component only (IP). We stress that E1013−477 is found below the line with the other IPs.

From the above discussion, a clear picture emerges in which the source E1013−477 seems to be a good, although anomalous, IP candidate. However, some inconsistencies are found in our data, as we now discuss.

We have compared the gross optical and X-ray properties of E1013−477 with those of other known hard X-ray sources. Patterson & Raymond (1985; hereafter PR) have investigated the emission of a sample of cataclysmic variables, accreting through a disk, using data accumulated by the *Einstein Observatory* IPC and their visual magnitudes. The sample includes five IPs and the two DQ Her systems known. In order to compare the optical and X-ray properties of E1013−477 to those reported by PR, we have measured the optical flux, F_V, in the range (5000–6000 Å) and the X-ray flux, F_x, in the range (0.2–4.0 keV). Our fit parameters (see §§ 2.3.2 and 4.3.2) imply $F_V = 0.23 \times 10^{-12}$ ergs cm^{-2} s^{-1} and $F_x = 0.28 \times 10^{-11}$ ergs cm^{-2} s^{-1}. PR plotted log F_x versus log F_V and found an upper bound to the distribution of the objects, corresponding to $F_x/F_V \sim 4$. The position occupied by E1013−477 in this diagram is extreme, violating the upper bound. Its rather high F_x/F_V ratio seems, instead, comparable to that found in some AM Her systems (Cordova & Mason 1983), excluded from the sample of PR. We must stress, however, that the optical flux is derived from data not simultaneous with the X-ray observations and that the V photometric measurements obtained during the X-ray observations are greater by a factor 30% than the average spectrum. Moreover, the average of the 20 spectra obtained on March 30 is fainter by the same factor than the spectrum obtained 1 day before.

We have also compared the ratio of the UV flux to the hard X-ray one (~ 1.1) with the values observed in IPs (0.48–8.5; Bonnet-Bidaud & Mouchet 1988). Only one source (GK Per in quiescence) has a ratio lower than E1013−477. From this point of view too, this source differs from IPs.

In summary, on the basis of its X-ray properties, E1013−477 looks like an IP. Our optical spectroscopy allows us to confirm the orbital period of 10.12 hr. Nevertheless, no spin period can be derived from our set of data. A larger body of observational data is needed to fully understand the nature of this source and solve problems such as the unobserved spin period.

Useful information was provided by the *EXOSAT* astronomical data base. This research made use of the SIMBAD data base, operated at CDS, Strasbourg, France. R. M. S. warmly acknowledges Joe Pesce for useful comments about the manuscript and for his valuable help in preparing the tables. Jan van Paradijs is thanked for his careful reading of the paper.

REFERENCES

Bailey, J. 1991, MNRAS, 243, 57
Barrett, P., O'Donoghue, D., & Warner, B. 1988, MNRAS, 233, 759
Berriman, G. 1988, in Polarized Radiation of Circumstellar Origin, ed. G. V. Coyne, A. M. Magalhaes, A. F. J. Moffat, R. E. Schulte-Ladbeck, S. Tapia, & D. T. Wickramasinghe (Vatican City: Vatican Obs.), 281
Bessell, M. S. 1979, PASP, 91, 589
Beuermann, K. 1988, in Polarized Radiation of Circumstellar Origin, ed. G. V. Coyne, A. M. Magalhaes, A. F. J. Moffat, R. E. Schulte-Ladbeck, S. Tapia, & D. T. Wickramasinghe (Vatican City: Vatican Obs.), 125
Boggess, A., et al. 1978, Nature, 275, 1
Bond, H. E., & Chanmugam, G. 1982, in Advances in Ultraviolet Astronomy: Four Years of *IUE* Research, NASA CP 2238, 530
Bonnet-Bidaud, J. M., & Mouchet, M. 1988, in A Decade of UV Astronomy with the *IUE* Satellite, ed. N. Longdon & E. J. Rolfe, ESA SP-281 (Greenbelt: NASA), 271
Chiappetti, L., Maraschi, L., Sambruna, R. M., & Treves, A. 1989, in Proc. 23 ESLAB Symp., Two Topics in X-Ray Astronomy, ESA SP-296 (Bologna: ESA), 349 (CMST)
Cordova, F. A., Jensen, K. A., & Nugent, J. J. 1981, MNRAS, 196, 1
Cordova, F. A., & Mason, K. O. 1983, in Accretion-driven Stellar X-Ray Sources, ed. W. H. G. Lewin & E. P. J. van den Heuvel (Cambridge Univ. Press), 147
Cropper, M. 1986, MNRAS, 222, 225
Echevarria, J. 1988, MNRAS, 233, 513
EXOSAT Observatory. 1991, The *EXOSAT* Data Base System, ESA TM-12, ed. C. Barron, ESA Pub. Div
Ferraz-Mello, S. 1981, AJ, 86, 619
Garnavich, P., & Szkody, P. 1988, PASP, 100, 1522
Hameury, J. M., King, A. R., & Lasota, J. P. 1989, MNRAS, 237, 845
Kubiak, M., & Krzeminski, W. 1989, PASP, 641, 669
Lamb, D. Q. 1985, in Cataclysmic Variables and Low-Mass X-Ray Binaries, ed. D. Q. Lamb & J. Patterson (Dordrecht: Reidel), 179
Lamb, D. Q., & Masters, A. R. 1979, ApJ, 234, L117
Lamb, D. Q., & Melia, F. 1987, Ap&SS, 131, 511
Maraschi, L., et al. 1984, in Proc. 4th European *IUE* Conf. ESA SP-218, 427
Mason, K., et al. 1982, *IAU* Circ. No., 3684
Mason, K., Cordova, F., Middleditch, J., Reichert, G., Bowyer, S., Murdin, P., & Clark, D. 1983, PASP, 95, 370
Morrison, R., & McCammon, D. 1983, ApJ, 270, 119
Mouchet, M., van Amerongen, S. F., Bonnet-Bidaud, J. M., & Osborne, J. P. 1987, Ap&SS, 131, 613
Mukai, K., & Corbet, R. H. D. 1987, PASP, 99, 149
———. 1991, ApJ, 378, 701 (MC)
Nugent, J. J., et al. 1983, ApJS, 51, 1
Paresce, F. 1984, AJ, 89, 1022
Patterson, J. 1984, ApJS, 54, 443
Patterson, J., & Raymond, J. C. 1985, ApJ, 292, 535 (PR)
Scargle, J. D. 1982, ApJ, 263, 835
Schmidt, G. D. 1989, in IAU Coll. 114, Magnetic Fields in White Dwards, ed. G. Wegner (Berlin: Springer), 305
Schrivjer, J., et al. 1985, Space Sci. Rev., 40, 121
Seaton, M. J. 1979, MNRAS, 187, 73P
Szkody, P. 1986, ApJ, 301, L29
Urry, M., & Reichert, G. 1988, *IUE* NASA Newsletter N.34
van der Woerd, H. 1987, Ap&SS, 130, 225
Voikhanskaja, N. F. 1987, Soviet Astron. Lett., 13(4), 250
———. 1988, A&A, 192, 128
Warner, B. 1983, in Cataclysmic Variables and Related Objects, ed. M. Livio & G. Shaviv (Dordrecht: Reidel), 155
———. 1986, MNRAS, 219, 347
Warner, B., & Wickramasinghe, D. T. 1991, MNRAS, 24, 370
White, N. E., & Peacock, A. 1988, Mem. Soc. Astron. Ital., 8, 7